UC Santa Barbara

UC Santa Barbara Electronic Theses and Dissertations

Title

Design and Application of a Microdialysis Fluorescence System to Simulate Root Exudation and Spatially Capture Soil-Microbe pCO2 Dynamics

Permalink

https://escholarship.org/uc/item/9ct2v630

Author

Navarrette, Maxi

Publication Date

2023

Peer reviewed|Thesis/dissertation

UNIVERSITY OF CALIFORNIA

Santa Barbara

Design and Application of a Microdialysis Fluorescence System to Simulate Root Exudation

and Spatially Capture Soil-Microbe pCO$_2$ Dynamics

A Thesis submitted in partial satisfaction of the

requirements of the degree Master of Sciences

in Ecology, Evolution, and Marine Biology

by

Maxi Navarrette

Committee in charge:

Professor Joshua Schimel, Chair

Professor John Melack

Professor Jennifer King

March 2023

The thesis of Maxi Navarrette is approved.

———————————————————

John Melack

———————————————————

Jennifer King

———————————————————

Joshua Schimel, Committee Chair

March 2023

ACKNOWLEDGEMENTS:

ABSTRACT

Design and Application of a Microdialysis Fluorescence System to Simulate Root Exudation

and Spatially Capture Soil-Microbe $p\mathrm{CO}_2$ Dynamics

by

Maxi Navarrette

Soil processes govern the largest terrestrial carbon pool, but describing the complex mechanisms that control these processes has proven difficult. A soil region particularly important to terrestrial C cycling is the rhizosphere and its underlying mechanisms. Rhizosphere mechanisms are complicated to experimentally capture because their spatial and temporal micro-scale (μm - cm) dynamics fall outside of the methodological reach of traditional experimental techniques. By employing microdialysis to simulate rhizosphere dynamics and simultaneously observing $p\mathrm{CO}_2$ with the non-toxic and stable fluorophore 8-hydroxypyrene-1,3,6-trisulfonic acid (HPTS), we are able to simplify and explore otherwise complicated microbial processes in a manner that minimizes disturbances. With the microdialysis system, an area of increased respiration around the microdialysis tip was successfully established and measured in the majority of replicates in a 24 hr time-series via a ratiometric fluorescence analysis. Because this method allows for the simulation of root exudation and analysis of subsequent microbial activity, it is a potential tool to study rhizosphere processes in a laboratory setting, though further development is needed.

1.   Introduction

Soil C decomposition is a function of microbial activity and of various soil properties, such as nutrient availability, temperature, moisture content, structure, and texture (Blagodatsky et al., 2010; Chen et al., 2014; Hicks Pries et al., 2015; Ronn et al., 2022; Silver et al., 2000; Vogel et al., 2015). Mechanistic description of these properties and processes is complicated due to their enmeshed nature (Seaton et al., 2020), intensifying or mitigating their impact on soil processes such as soil organic matter (SOM) stabilization or decomposition (Lauber et al., 2008).

Microbial community activation is as much a function of macro-scale inputs such as rainfall, vertebrate decomposition (Keenan et al., 2018), and litter decay (Dowdy, 2021) as it is a function of small-scale properties such as soil structure and texture (Kaye et al., 2002). For example, certain mineral assemblages and soil structures form preferential flow pathways, enriching micro-sites with water and nutrients as their diffusion is mediated by water, activating microbial populations (Grant et al., 2019). Additionally, organo-mineral complexes may partition carbon away from microbially-accessible pools into mineral associated organic matter (MAOM) pools, constraining SOM decomposition (Sulman et al., 2014). If microbes do not have access to labile carbon or the necessary exoenzymes to exploit more recalcitrant stores of SOM, then microbial populations will become inactive (Gochun, 1987). Alternatively, some soil microsites will experience increases in microbial activity if soil pathways promote needed water and nutrients flows. Because of the micro-scale variations in soil structure, regions of microbial community activation and inactivation may be separated by mere micrometers (Kuzyakov & Blagodatskaya, 2015).

1

An area of particular interest and complexity is the soil-microbial-root matrix, termed the rhizosphere. The rhizosphere is often considered a 'hotspot' of microbial activity compared to the majority of the soil volume (Kuzyakov & Blagodatskaya, 2015). The rhizosphere hosts populations of microbes that are up to 32 times larger than in soil space devoid of roots (Kuzyakov, 2002), resulting in faster soil processing rates (Garcia et al., 2005) and thus significantly elevated rates of SOM turnover (Kuzyakov, 2002). Many of the elevated soil microbial processes in the rhizosphere are fueled by the continuous and high amount of organic matter input to the rhizosphere (Garcia et al., 2005). As much as 15% - 25% of below ground C allocation is perfused as soil labile C (Kuzyakov, 2002). Hence, the energy limitations that typically constrain microbial activity in mineral soil are reduced in the rhizosphere (Canarini et al., 2019; Clarholm, 1981; Kuzyakov, 2002).

Rhizosphere dynamics have been studied for the past 40 years, though descriptions of rhizosphere mechanisms remain incomplete because of the complicated spatial and temporal nature of roots and root exudation (König et al., 2022). Root exudates diffuse primarily from the root-tip rather than the entire root-length, so microbial community activation is spatially constrained to the portion of the rhizosphere associated with the root terminus (Canarini et al., 2019; König et al., 2022). Roots exude a broad suite of molecular compounds that have varying effects on microbial activity and SOM decomposition. They exude tannins which can immobilize extracellular enzymes or their substrates (Fierer et al., 2001; Kraus et al., 2004), and so inhibit decomposition. They also exude polysaccharides (mucilage) that promote soil aggregation by physically protecting SOM from microbial decomposition and establishing liquid-water bridges (Bardgett et al., 2014; Carminati et al., 2017). Perhaps the most obvious way roots influence microbial activity is via exudation of labile C in the form of

monosaccharides to the rhizosphere (de Graaff et al., 2010). However, the way that soil microbes respond to simple sugar inputs remains complicated. Depending on nutrient availability, labile C inputs may encourage microbes to either exploit SOM or to not do so in favor of the simple sugar rhizodeposits (Garcia et al., 2005), though thresholds of specific nutrient availability and soil conditions that prompt either of these microbial life strategies are not well defined (Chen et al., 2014; Kuzyakov, 2010).

Additionally, as roots extend through soil, hotspots of carbon and accessory chemical deposition will change throughout the soil profile, stimulating soil processes in some regions while the process rates of previous hotspots slow (Canarini et al., 2019). Furthermore, exudate quantity and carbon concentration change both seasonally and as a function of plant age (Aulakh et al., 2001; Swann 2018), complicating rhizosphere dynamics. The spatial and temporal properties of root exudation contribute to the complexity of rhizosphere processes, making them difficult to study with the tools currently available (Kuzyakov & Blagodatskaya, 2015).

Rhizosphere Tools:

To paint a microbially and biogeochemically-relevant picture of rhizosphere processes, experimental methods must be able to capture micro-scale and spatially dynamic processes as a function of time. Consequently, our current suite of tools falls short (König et al., 2022). Many conventional techniques require physically mixing or sieving samples; doing so disrupts soil structure and incorporates nutrients throughout the soil which shift microbial dynamics (Ettema, 2002; Hobbie & Hobbie, 2013; Inselsbacher et al., 2014). The methodological emphasis on soil averaging via compositing soil replicates and sieving has

been largely intentional. Heterogeneity has, for the most part, been viewed as random and thus an obstacle to overcome through homogenization and replication. Few studies have explored micro-structure as a soil property that may have macro-scale implications (Smercina et al., 2021). Previous investigations into the impact of labile C input on microbial response have applied labile C as a solution on top of the soil profile or mixed nutrients and sugars into soils (Broadbent & Norman, 1947; König et al., 2022; Kuzyakov et al., 2000). These experimental approaches altered mass flow in soil or disrupted the soil structure, possibly altering microbial processes (Grossmann & Udluft, 1991; König et al., 2022). If observing microbial processes *in situ* is the aim, clearly these are inappropriate means. Non-destructive, micro-scale oriented techniques like soil zymography are now available and allow for non-destructive micro-scale experiments, although they have yet to be systematically applied to soils (Baveye et al., 2018; Spohn & Kuzyakov, 2013).

This investigation aims to develop a method that packages two existing technologies together—microdialysis and 8-hydroxypyrene-1,3,6-trisulfonic acid (HPTS), a pCO_2 sensitive fluorophore— to facilitate the study of the relationships between root exudation and microbial activity. Microdialysis (MD) enables the collection of solutes at the micrometer to centimeter scales relevant to rhizosphere processes *in situ* and with minimal disturbance to surrounding soil structures (Kho et al., 2017). Through passive diffusion, analytes of interest cross a membrane barrier in the microdialysis probe, effectively taking a snapshot of solution chemistry (König et al., 2022). Microdialysis has been successfully applied to soil systems to study low molecular weight organic carbon (Randewig et al., 2019) and root uptake dynamics of phosphate, as the technology is capable of replicating soil P dynamics by mimicking the diffusive gradients that roots establish (Demand et al., 2017). The technology

has also been used to examine amino acid dynamics in tundra plants with promising results (Homyak et al., 2021).

An inversion of microdialysis is retrodialysis. Here, glucose or other low molecular weight compounds are pumped through the microdialysis probe, creating a diffusion gradient from the probe into the soil. This approach introduces the chemical of choice into the surrounding soil through passive diffusion (König et al., 2022). In this way, a microdialysis probe can act as an artificial root simulating rhizosphere dynamics in the soil immediately surrounding the probe.

The virtue of this system is its simplicity. Real world root systems are messy—mucilage, dead root tips, and other accessory root exudates like tannins that may inhibit microbial activity make it difficult to experimentally determine the impact of labile C fluxes on microbial activity (Fontaine et al., 2003; Ushio et al., 2013). Roots also alter moisture and oxygen dynamics in the rhizosphere (Blossfeld et al., 2011). Microdialysis allows scientists to isolate root-exudation without the complicating activity of other roots. Because of its simplicity compared to real systems, retrodialysis offers scientists an opportunity to simulate root exudation without the other activity of live roots at relevant scales in a way that minimizes disturbance.

In this study, microdialysis will be used in conjunction with HPTS, a non-toxic hydrophilic and water soluble fluorophore that changes fluorescence intensity in response to pH shifts. Because of its pH responsiveness, it can be used to spatially map $p\text{CO}_2$ concentrations in the soil as dissolved CO_2 causes pH shifts by forming carbonic acid (Zhu et al., 2006). Because the majority of $p\text{CO}_2$ efflux in soil is sourced by soil microbes, the distribution of CO_2 in the soil can be seen as an optical proxy of microbial activity. Due to

these qualities and the sufficiently wide distance between its excitation and emission spectra (its Stoke's shift) HPTS is commonly used to study pH and pCO_2. Many alternative fluorophores are toxic or show inferior Stoke's shifts, limiting their use (Alford et al., 2009). Most recent studies that have employed the fluorophore HPTS have focused on sediments and have done so by entrapping HPTS onto thin supporting sheets of plastic—a technology termed "planar optodes" (Glud et al., 1996; Larsen et al., 2011; Li et al., 2019; Zhu & Aller, 2010). The lure of planar optodes as a vehicle for fluorophores is evident: they are stable, solid-state, and reusable (Blossfeld et al., 2011; Holz et al., 2020; Lenzewski et al., 2018). However, their fabrication process is complicated and requires the use of organic solvents and plastics (Zhu & Aller, 2010). Additionally, as they are plastered onto a plastic sheet, they cannot directly associate with the actual root and soil structures they intend to study. No studies have attempted to apply the fluorophore HPTS to soil contexts as an aqueous solution, which is surprising as HPTS is stable, and easy to both prepare and apply. Importantly, it may also allow for tighter soil-fluorophore associations yielding more microbially relevant pCO_2 analyte data.

The objective of this study is to investigate the direct application of $HPTS_{(aq)}$ to soil as a method for detecting CO_2 resulting from microbial respiration of perfused glucose solution introduced through retrodialysis. This approach has the potential to significantly expand observational capabilities in studies of rhizosphere processes.

2. Methods

Rhizobox:

Each rhizobox was constructed of 0.635 cm thick acrylic. Acrylic sheets were cut into square pieces of an area of approximately 12 cm^2. Acrylic was chosen for its mix of

durability, superior optical clarity, and low cost. These square pieces were bonded to each other at their edges using an acrylic cement to form the rhizoboxes. For the majority of bonding (acrylic box sides and the non-viewing bottom edge) a liquid acrylic cement was employed. An acrylic cement gel was used for the viewing face A (Fig. 1).
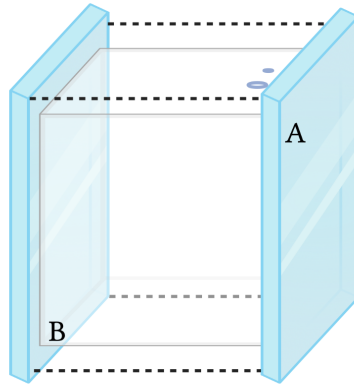
Figure 1: The viewing face of the rhizobox is side A. Side A has a smaller but congruent square of acrylic joined to its underside to facilitate water-retention. Side A was cut to be slightly bigger than the rest of the side pieces so that it could be attached and tightened to the bottom piece (also cut to be slightly bigger) which is represented as the same teal color as side A connected to it with the dotted lines which represent the fastener called All-Thread on all four corners. B represents the side faces of the acrylics box of which there are four. In all there are six sides, the top and bottom and the four side pieces.

Watertightness was ensured through use of a closed - cell gasket and through ample tightening of the viewing edge to the rest of the box with four zinc plated All-Thread Rods of 0.93 cm diameter drilled through each corner of viewing edge A into the bottom of the box. Two holes were then drilled into box sides (Fig. 1). The first was 1 mm in diameter to allow for the 0.5 mm diameter Harvard Biotech Sciences microdialysis probe to fit through. This hole was placed as near the viewing edge as possible so that it would be visible to the camera when the boxes were filled with soil (Fig. 2). A second hole was placed on the side face to accommodate a septum to facilitate extraction of liquid for the calibration.

A very fine, sandy loam identified as Mollic Palexeralf of the Milpitas series was collected from UCSB campus. A 20 x 15 cm pit was dug, and the soil from the pit was then shoveled into 6 laboratory-constructed rhizoboxes. While this collection method disturbed soil structure, care was taken to preserve aggregates and native soil elements such as roots, rocks, and litter. By the end of the collection process each box contained a 12 cm cubed volume of soil. Soil boxes were covered with Saran wrap and brought into the lab where they were kept covered and shielded from sunlight until used for experimentation.
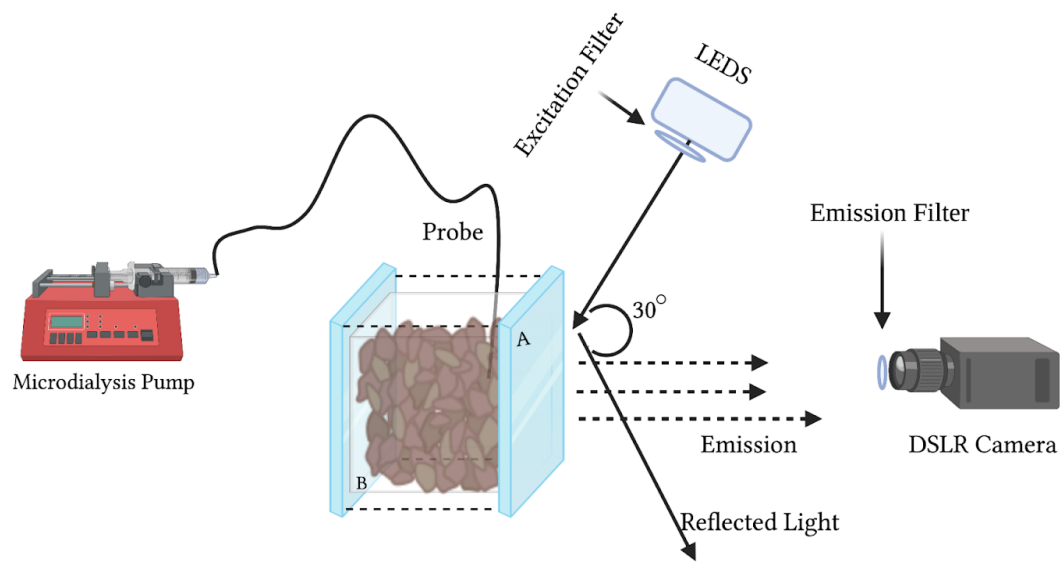
Figure 2: Schematic of complete experimental set-up. Soil solution is coated with free-HPTS. Both LEDs were fastened above the viewing box. Excitation filters were placed in front of LEDs. An emission filter was placed in front of the DSLR camera. Functioning together, the microdialysis pump perfuses glucose at 40 µg/mL into the rhizobox, and the DSLR + LED set-up collects images of subsequent dynamics.

HPTS Fluorescence:

A 40 μM stock solution of HPTS was made by mixing the fluorophore with water. This concentration was chosen because it had good fluorescence underneath the lighting configuration (Fig. 2) and previous investigations have successfully studied pH dependent fluorescence of free - HPTS at similar concentrations (de Nooijer et al., 2008). HPTS (21.9 mg) was mixed with 1L of water and stirred until the HPTS was fully dissolved. The HPTS solution had a pale green tint in indirect sunlight and bright fluorescence underneath 405 nm light.

Excitation Light and Filter Settings and Optics and Electronics:

For excitation of the CO_2 fluorophore, one high powered blue LED (wavelength peak = 465 nm, radiant flux of 930 mW, XPEBRY-L1-0000-00R01-SB01) and one high powered UV LED (wavelength = 405 nm, radiant flux is 625 mW, LST1-01G01-UV04-00) were used.

A NIKON D5600 DSLR camera was used to capture fluorescent images. It has an optical resolution of 24.2 million pixels and a sensor size of 23.5 x 15.6 mm. Camera shutter time was set to 3 s, and ISO was fixed to 100. A Micro NIKKOR 105 mm macro lens was used for its ability to capture very small objects with high resolution and its 1:1 focus ratio which minimizes distortion.

Bandpass filters were mounted onto both light sources and the camera: a 520 nm MIDOPT bandpass filter was affixed to the camera, while a 405 nm and a 472 nm Alluxa bandpass filter was placed in front of the 405 nm and 465 nm high powered LEDs, respectively (Fig. 2). The LEDs were wired to a Konrad power supply unit and manually powered on and off during image acquisition. The UV 405 nm LED was driven at 350 mA while the blue 465 nm LED was driven at 500 mA.

Images were captured as RAW image files and later analyzed in ImageJ. A ratio was taken between each pixel in the UV and blue images.

System Set-Up:

The complete experimental set-up combined the aforementioned elements of the microdialysis system, fluorophore, and a rhizobox (Fig. 2). The rhizobox was secured on a lab bench. Two LEDs with respective irradiation maximas of 405 nm and 465 nm were fixed above the rhizo-fluorescence system at 60 degrees from horizon so that incident light would glance off the sensing membrane and acrylic box at 30 degrees. A camera was placed in front of the acrylic box parallel to the excitation light emitted from the fluorosensor. In this way, unwanted light from the LEDs was minimized while excitation light reaching the camera was maximized, optimizing the captured signal. The microdialysis pump was placed behind the rig with the probe threaded through the microdialysis port hole into the moist soil. Care needed to be taken when inserting the probe into the soil; the probes (30 mm in length) are delicate and prone to breaking.

Calibration:

To correlate pixel intensity in ratio images to actual pCO$_2$ values, a 20 µM solution of HPTS was prepared by mixing 12.6 g HPTS into 1.2 L of water for 5 minutes. The 20 µM solution was used for calibration instead of the 40 µM solution, as fluorescence intensity in pure water was too high at the original concentration, saturating the camera's sensor. Concentrations of HPTS were kept at 40 µM for the rest of the experiment. For the same reason, camera exposure time was reduced to 1 second. The calibration curve was determined to be applicable to the study system despite these changes, because reductions in

fluorophore concentration and camera exposure time resulted in linear decreases in intensity. The ratiometric method of fluorescent image analysis employed in this study to quantify $p\text{CO}_2$ is robust to linear shifts in fluorescence (Zhu 2010). Then, a volume of 200 mL of the HPTS solution was placed in the rhizobox. After, a 5% CO_2 gas mixture balanced with nitrogen was bubbled through the water column for 0 seconds, 2.5 minutes, or 5 minutes in the rhizoboxes. Fluorophore emission was captured by the DSLR camera upon exposure to either the UV or blue light. The process was then repeated for the

$$y = 0.32 - 2.41 \times 10^{-5}\, x,\ R^2 = 0.97$$
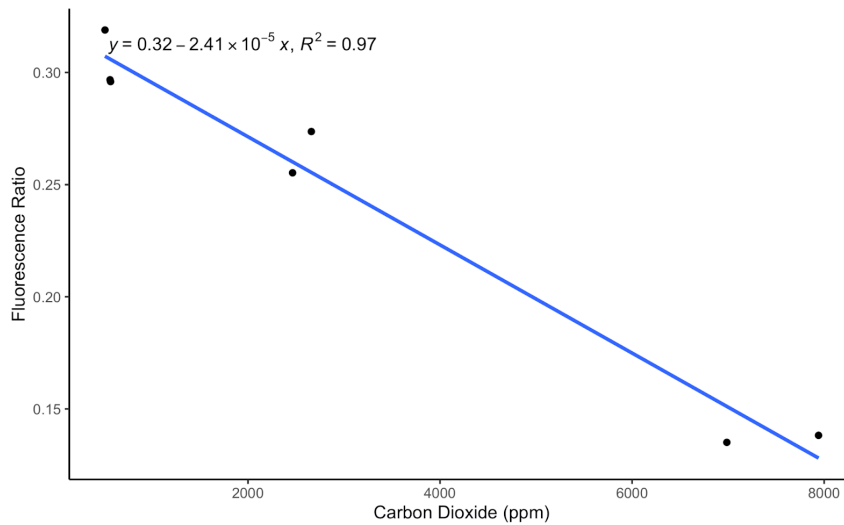
Figure 3: Calibration curve of blue/UV light ratio to carbon dioxide. Equation of the line was determined with the R package *ggpmisc* (Aphalo 2022).

next light. After fluorescent imaging, 50 mL of the free-HPTS solution was removed from the rhizobox through the septum. It was then injected into a sealed glass jar (100 mL volume) and shaken vigorously for 2 minutes to equilibrate water and gaseous carbon dioxide concentrations per the bottle calibration method outlined by Johnson et al. (1990). The CO_2 concentration of the jar headspace was then quantified using an infrared gas analyzer (LiCOR Biosciences Li820). $p\text{CO}_2$ in the solution was then back calculated using Henry's

law (Enick 1990). A calibration curve was then established relating concentration of CO_2 to the ratio of fluorescent intensity between the UV and blue lights (Fig. 3).

Image analysis:

Images were analyzed ratiometrically. Fluorescent excitation intensity of rhizobox soils following exposure to UV light was captured by the DSLR camera and then compared to fluorescent excitation intensity following exposure to blue light in ImageJ. Because UV fluorescence intensity increased as a function of increasing pCO_2, darker regions in the images are regions of higher pCO_2 concentration (Fig. 3). This method is intended as a tool to enable scientists to qualitatively identify regions of higher pCO_2 concentration, a by-product of microbial metabolism of the glucose perfused into the rhizobox. As a qualitative, spatial tool, ascertaining exact concentrations of pCO_2 was considered outside of the scope of this study. Blue excitation images were divided by UV images pixel by pixel to produce the ratiometric image. All images presented in this work are ratiometric images unless otherwise stated.

Ratiometric images collected through time show changes in relative CO_2 concentrations and reflect microbial activity, as indicated by increases in CO_2 concentrations.. An object of particular interest in this study was the rhizosphere halo. The rhizosphere halo is a concentrated region of microbial activity surrounding the probe tip from where glucose is diffusing. Because of the diffusion patterns of both glucose and carbon dioxide through soil as a function of macro and micro-pore pathways, the region of elevated microbial activity often takes the shape of a halo (an oval region of activity around the probe). Analysis and interpretation of images is performed in light of this crucial

soil-rhizosphere phenomena as it is representative of microbial metabolism of rhizodeposits. The data are intended to illustrate the establishment and growth of a halo through time as a result of the glucose perfused into the system through the microdialysis probe.

a. *Rhizosphere Simulation Benchmark:*

If pixel intensity (PI) around the probe was at minimum 50% lower relative to average background fluorescence, it was deemed that elevated microbial activity was a product of simulated root exudation (Table 1; Table 2). Benchmarking this way ensured standardization between time points so that the evolution of the carbon dioxide halo around the microdialysis probe could be consistently tracked.

Sample	Time Points (hrs)	Background Fluorescence (PI)	Halo Threshold Ratio (PI)
R1	0.0	0.7444	0.3722
R1	7.5	0.7802	0.3901
R1	24.0	0.7040	0.3520
R1	30.0	0.7136	0.3568
R2	0.0	0.5662	0.2831
R2	7.5	0.8166	0.4083
R2	24.0	1.2714	0.6357
R2	30.0	0.5832	0.2916
R3	0.0	0.7338	0.3669
R3	7.5	1.4686	0.7343
R3	24.0	1.9016	0.9508
R3	30.0	0.8244	0.4122
R4	0.0	1.0424	0.5212
R4	7.5	1.0502	0.5251
R4	24.0	1.0648	0.5324
R4	30.0	0.9916	0.4958

Table 1: Treatment table shows the average Background Fluorescence via pixel intensity for all time points and treatment replicates. PI stands for pixel intensity. The column Halo Threshold Ratio (PI) refers to the 50% pixel threshold that was used as the benchmark for microbial halo determination. If regions around the probe showed a lower ratio than the Halo Threshold Ratio then that region could be categorized as a rhizosphere halo; if the region exceeded the Halo Threshold Ratio, that region could not be categorized as a rhizosphere halo.

Sample	Time Points (hrs)	Background Fluorescence (PI)	Halo Threshold Ratio (PI)
C1	0.0	0.8260	0.4130
C1	0.5	0.9120	0.4560
C1	7.5	1.4598	0.7299
C1	24.0	2.0402	1.0201
C2	0.0	0.7160	0.3580
C2	0.5	0.6708	0.3354
C2	7.5	0.5496	0.2748
C2	24.0	0.5926	0.2963

Table 2: Control table shows the average Background Fluorescence via pixel intensity for all time points and treatment replicates. PI refers to pixel intensity. The column Halo Threshold Ratio (PI) refers to the 50% pixel threshold that was used as the benchmark for microbial halo determination. If regions around the probe showed a lower ratio than the Halo Threshold Ratio, then that region could be categorized as a rhizosphere halo; if the region exceeded the Halo Threshold Ratio, that region could not be categorized as a rhizosphere halo.

b.   Microbial Halo Size Determination:

The moistened soils were prone to settling over the 24 hour measurement. Figure 4 illustrates the movement of soil downwards from the 7.5 hr to 24 hr time point, revealing more and more of the microdialysis probe. In most cases, the revealed section of the probe would meet the minimum pixel intensity benchmark, but would not be indicative of a growing region of elevated microbial activity (rhizosphere halo). Thus, to accurately determine the rhizosphere halo size as a function of respiration and not soil settling, the halo was measured by width, not area.
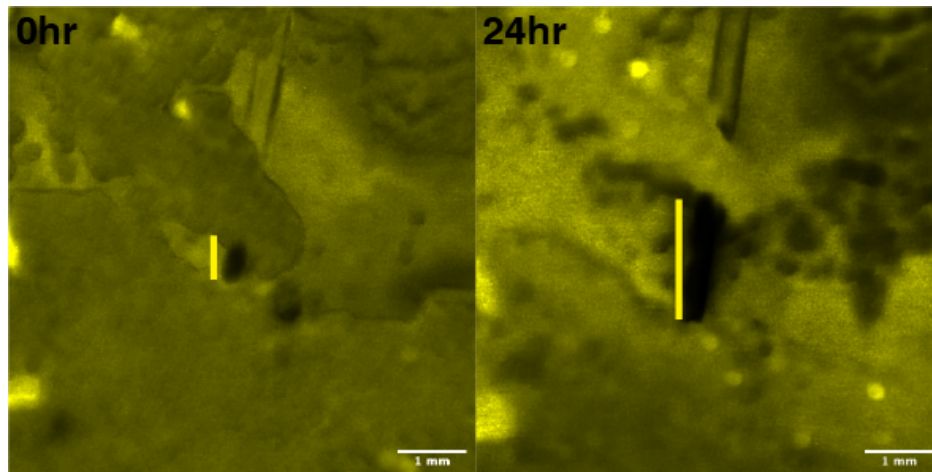
Fig. 4: Between the 0 hr and 24 hr time point in R2 there is significant settling of the soils, such that more of the microdialysis probe length is revealed over time. The yellow vertical bar placed just the left of the probe illustrates soil settling from time point 0 to time point 24. In the 24 hr period, the visible probe surface grew just under 1 mm to ~1.5 mm as a function of soil movement.

Width was calculated by measuring from the probe edge outwards in the x-direction (Fig. 5). This measurement system was chosen to avoid measurement error due to halo asymmetry and to avoid sampling width of the microdialysis probe itself. Finally, color differences visible between replicates are due to proximity of sediments to wall face, but had no impact on analysis (Fig. 5a,b).

Experiment: *Root Simulation*

        Soils were re-wet with HPTS to 60% volumetric water content. Soils were given 30 minutes for the solution to distribute throughout the soil profile and then the viewing face was fixed to the acrylic box sealing it. The rhizobox was then placed on its face for 15 minutes so that the HPTS solution would coat the soils closest to the viewing edge. Afterwards, soils were deemed ready for fluorescence imaging.

        Root simulation was achieved with a CMA Harvard Biotech Microdialysis pump, 30 mm Harvard Biotech microdialysis probe, and a 5 mL syringe (Fig. 1). The experimental

15

design involved a high glucose treatment (4 replicates) and a control (2 replicates). In the high glucose treatment, rhizoboxes received a 5 mL perfusion of glucose of 40 µg/ml concentration through the microdialysis probe. The control received a 5 mL perfusion of purified water (< 18 Ohm; Millipore Milli-Q lab water system). In both treatment and control, the 5 mL syringe was connected directly to the microdialysis probe with a tubing adapter also purchased from CMA. The adapter was soaked in ethanol for 10 minutes to facilitate attachment to the probe inlet and to the syringe tip. Regardless of concentration, the solution was perfused into the study system at the same speed (3.47 microliters per hour). Experiments were run for 24 hrs total — the microdialysis rig perfused 5 mL over that entire time period, and fluorescent imaging was performed at 0 hr, 1/2 hr, 7.5 hr, and 24 hr intervals. Image acquisition was performed in the same manner as the calibration. Experiments were performed on different days with the same imaging set-up over a period of two weeks. Storage and experimental conditions were kept temperature controlled at ~20°C. Microdialysis probes were reused if possible, but control probes were never used for high glucose treatment replicates and vice-versa. Additionally, if re-used, probes were allowed to completely air-dry before re-insertion to deactivate microbial communities on the probe surface and thus reduce legacy effects.

3.   Results & Discussion

The intent of this investigation was to spur microbial activity through microdialysis-supplied glucose and spatially identify subsequent soil carbon dioxide emissions with HPTS. This system would allow micro-scale exploration of root exudation and associated microbial activity in a controlled environment with known inputs. This technique is intended to address a growing need for low disturbance, temporally dynamic,

high resolution technologies to better understand the complicated and enmeshed rhizosphere processes that have been the focus of study in the soil sciences for more than 40 years. Using this experimental design, the concentration and type of root exudate that is perfused into the system can be controlled, allowing the exploration of micro-scale microbial responses to a wide range of compounds representative of root exudates. Localized effects produced by the microdialysis system could then be identified with HPTS.

Data were collected and analyzed to compare carbon dioxide dynamics in the rhizobox. While pixel intensities are correlated to carbon dioxide concentrations, the focus of this study was to map regions of high microbial activity around the microdialysis probe as a function of perfusion of glucose into the treatment box over time. To provide a rough estimate of CO_2 evolution given the treatment of 8.3 mg of glucose over 24 hours, a simple calculation was performed.

a. *CO_2 estimates:*

System CO_2 estimates were calculated as a function of glucose perfusion into the system, according to an existing model for carbon use and exoenzyme dynamics as follows (Schimel & Weintraub, 2003):

$$Glucose = 8.3 * 10^{-3} g$$
$$R_m = (Km * Glucose)$$
$$R_g = (Glucose - Rm)(1 - Sue)$$

where:

R_m : respiration to support energy needs

R_g : respiration to support growth of the microbial biomass

Sue : substrate use efficiency

K_m : microbial maintenance rate.

$$Glucose - R_m - R_g(1 - SUE) = 4.1 * 10^{-3}g \tag{1}$$

$$by : C_6H_{12}O_6 + 6O_2 -> 6CO_2 + 6H_2O \tag{2}$$
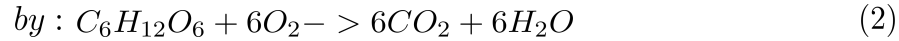
$$4.1 * 10^{-3}g_{C_6H_{12}O_6} * \frac{1mol_{C_6H_{12}O_6}}{180.156g_{C_6H_{12}O_6}} * \frac{6molCO_2}{1molC_6H_{12}O_6} * \frac{44.1gCO_2}{1molCO_2} = 5.9mgCO_2 \tag{3}$$

Over the 24 hour time series, the amount of CO_2 respired from the microdialysis glucose probe was expected to fall under this calculated maximum value of 5.9 mg CO_2. To simplify the calculation, it was assumed that enzyme synthesis and associated respiration would not occur, as glucose metabolism does not require enzymes. Substrate use efficiency was assigned a value of 0.5, consistent with measured values for carbohydrates (Schimel, 2003). Additionally, the microbial maintenance rate K_m was taken to be $0.022d^{-1}$ and was based on the number used to parameterize Schimel and Weintraub's 2003 exoenzyme model, whose model was parameterized with data from Vance and Chapin (Schimel & Weintraub, 2003; Vance & Chapin, 2001). This value was found to be appropriate to describe the study system because it assumes negligible microbial biomass growth. Due to the short time frame of the experiment, microbial communities were likely to still be activating, primarily allocating resources to support maintenance (Mondini, 2006)

a:Replicate 1
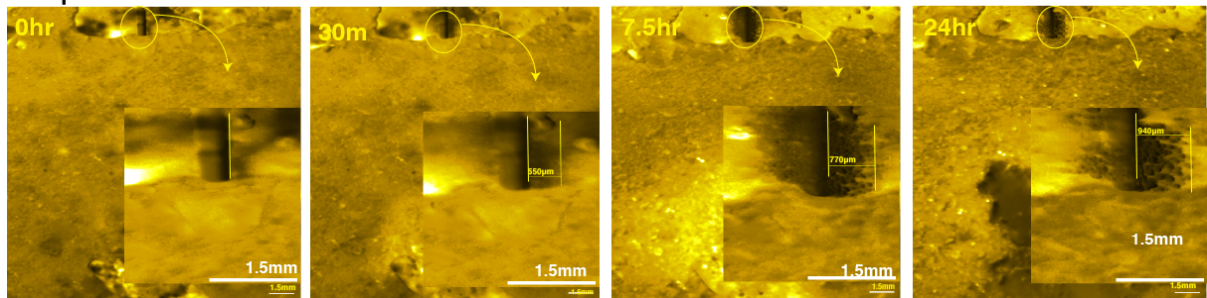
b: Replicate 2
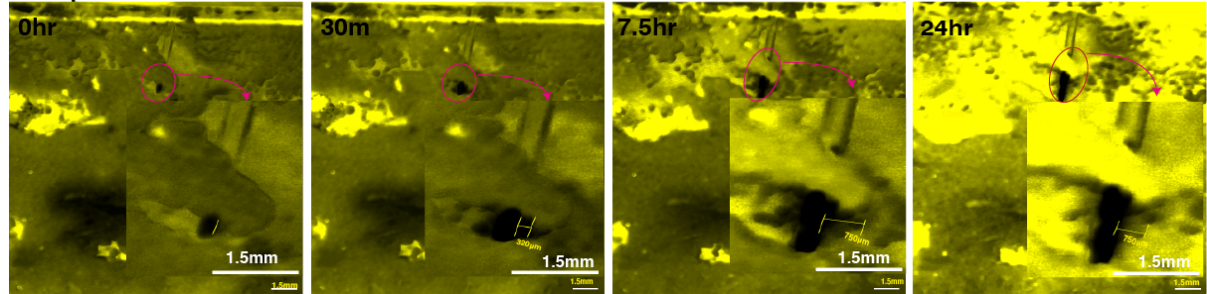
c: Replicate 3
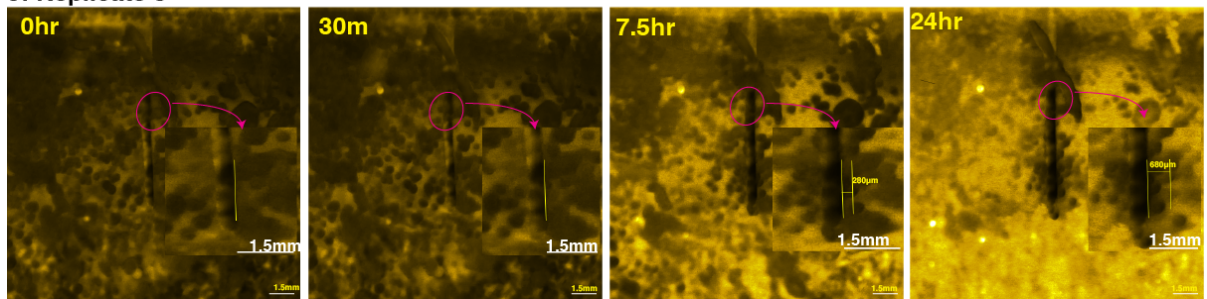
d: Replicate 4
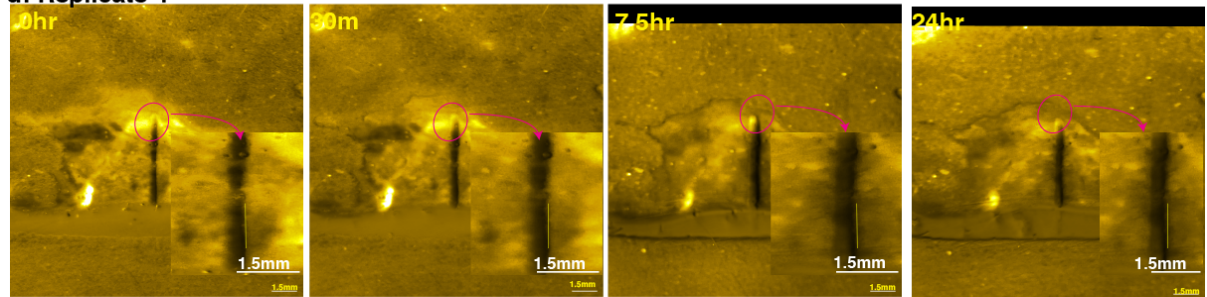
e: Control 1
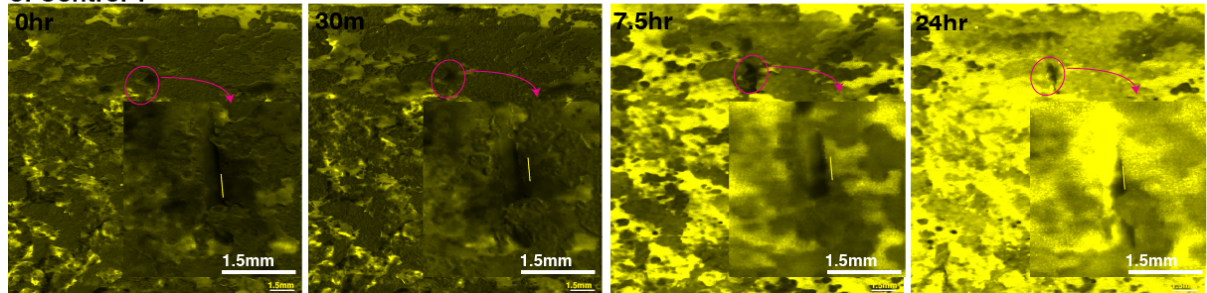
CO2 Legend (ppm)

low ——→high

19

Figure 5: Each panel follows a 24 hr time series, and showcases four timepoints: 0 hr, 1/2 hr, 7.5 hr, and 24 hour. The small-scale, larger image illustrates the probe's position in the rhizobox. The large scale overlays emphasize changing pCO$_2$ around the probe. Treatment panels include slim, yellow bars to illustrate the growth of halos of microbial activity around the probe as a function of time. The same yellow lines are included in control, but because no growth was observed they are static. A pCO$_2$ legend is included below to illustrate general pCO$_2$ trends.

b.   *Rhizosphere Halo & Perturbation Analysis*

Replicate one (R1) shows a progressive decrease in pixel intensity surrounding the microdialysis probe from 0 hr to 24 hrs (Fig. 5a). Between time zero and thirty minutes, the region of darker pixel intensity that exceeds the 50% background threshold grew to 550 μm and increased in size to 770 μm and 940 μm at the 7.5 hr and 24 hr time points, respectively (Fig. 5a). The R1 halo of elevated pCO$_2$ reaches a maximum width of 940 μm. The width of elevated pCO$_2$ corresponds with what is seen in natural rhizosphere systems, if on the lower end; because gas can diffuse through soil pore space, elevated carbon dioxide around roots has been identified up to 20,000 μm away from the root (Kuzyakov & Razavi, 2019). That the R1 halo reaches a maximum width of 940 μm at the end of the experiment is likely a function of the abbreviated nature of the experiment. Soil microbial dynamics are slow; maximum increases in respiration rates are often not observed until days after glucose amendment, so it may be that the experimental length was simply not long enough to fully capture potential rhizosphere dynamics around the probe (Blagodatsky et al., 2000). Additionally, the modest rhizosphere halo established in R1 may also be explained by the relatively high 60% volumetric water content (VWC) of study soils. As soils become increasingly saturated, gas diffusion is stymied because of high water-filled pore space, and increased compaction as a result of saturation minimizes possible flow pathways reducing the ability of gasses to diffuse (Currie 1984). The same dynamics that likely reduced the potential size of the halo of microbial activity around the probe likely impacted all replicates.

Finally, that we see elevated pCO_2 dynamics around the probe in R1 as well as R2 and R3 in the 24 hr period of this experiment is promising. Significantly, neither control showed evidence of elevated pCO_2 around the microdialysis probe (Fig. 5e, Fig. 6 Control).

Macro-scale perturbation events within the experiment highlighted the ability of microdialysis probes to simulate root exudation and establish a region of elevated pCO_2 around the probe. Briefly, perturbation was a function of soil mixing and wetting, both of which caused a short macro-scale pulse in respiration throughout the rhizobox, which corresponds with perturbation dynamics observed in other studies (Kuzyakov et al., 2000; Grossmann & Udluft, 1991). This pulse was visible in the control and both R2 and R3 as a general brightening of soil or increase in pixel intensity in the rhizobox in every time point from 0 to 24 (Fig. 5b-c & e), though the perturbation effect was not seen in R1 (Fig. 5a). The ability of HPTS to register sub-hourly pCO_2 dynamics is consistent with other experimental findings (Zhu, 2006; Zhu & Aller 2010; Larsen et al., 2011).

Notably, despite macro-scale pCO_2 decreases in the rhizobox for R2 and R3, the probes not only hosted regions persistently lower in pixel intensity than the 50% pixel intensity threshold benchmark for their respective time points, but that region grew over time for both replicates (Fig. 5b, c). This corroborates a finding by König (2022) which found through ^{13}C labeling that a significant portion of labile C introduced to soil was subsequently respired by microbes. It appears that microdialysis is capable of stimulating a region of significantly elevated microbial activity. On the other hand, in control rhizoboxes the pCO_2 in regions close to microdialysis probes were subject to macro-scale dynamics as the pixel ratio increased concomitantly with the rest of the soil volume (Fig. 5e; Table 2). Reviewing control and treatment probe dynamics in light of perturbation effects suggests that perfusion

of glucose with the microdialysis probe successfully established a micro-site of elevated

microbial activity. Not only was a region of elevated microbial activity established, its signal

was strong enough to be visible despite macro-scale perturbations (Fig. 5b). Additionally, the

strength of the signal despite macro-scale disturbances is evidence that microdialysis probe

dynamics in treatment are a function of glucose perfusion alone and not due to background

decomposition of leaf litter or sources of SOM in the soils.

While the R1 rhizobox did not host the same perturbation dynamics as the R2 and R3

rhizoboxes, the similarity between all three of these replicates despite macro-scale

differences increases certainty in the ability of microdialysis to produce a rhizosphere effect,

and legitimizes this study's application of HPTS as a method to visualize micro-scale

processes despite macroscale disturbances (Fig. 5a-c).
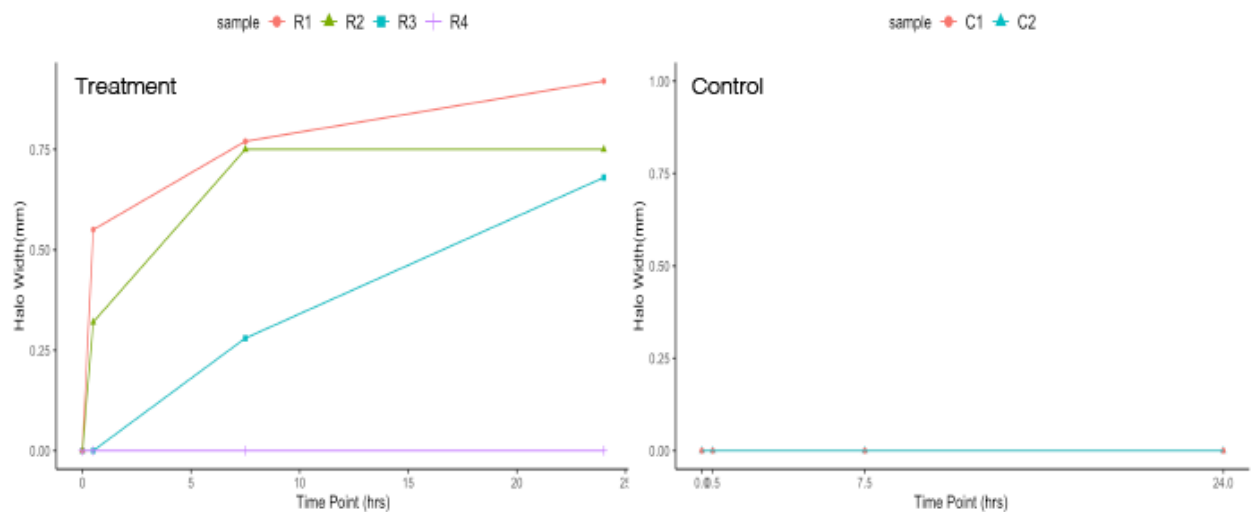
Figure 6.: Changing dynamics of treatment and control during 24 hr time series: Treatment: Illustrates halo width over 24 hrs. Replicates are differentiated by colored lines and symbols as indicated in the legend. The control is differentiated by color and shape in the same manner. R1-R3 shows growth in width of the halo surrounding the microdialysis probe. R4 shows no change over time. **Control:** Both controls showed the same static dynamics. No halo was observed to grow in either control.

Though replicates R1-3 showed similar dynamics around the probe, there was no significant increase in pCO$_2$ around the probe tip in R4 (Fig. 5a-d, Fig. 6 Treatment). Whether this was a function of improper probe placement or suggestive of method unreliability is unclear. Considering improper probe placement, some issues arose in the course of investigation; probes needed to be in contact with soil but not completely obscured to be useful. Threading the probes through the microdialysis port-hole was generally challenging, as probes were often obscured from view on insertion. The difficulty of insertion required many repeat attempts leading to probe breakage. Previous researchers have also noted their fragility (Buckley, 2020; Brackin et al. 2017). This occurred in R4, which may have led to a damaged membrane resulting in the control-like no effect (Fig. 5d, Fig. 7). Additionally, the R4 probe was inserted into a somewhat large air pocket that could be to blame for the lack of carbon dioxide production in the vicinity of the microdialysis probe.
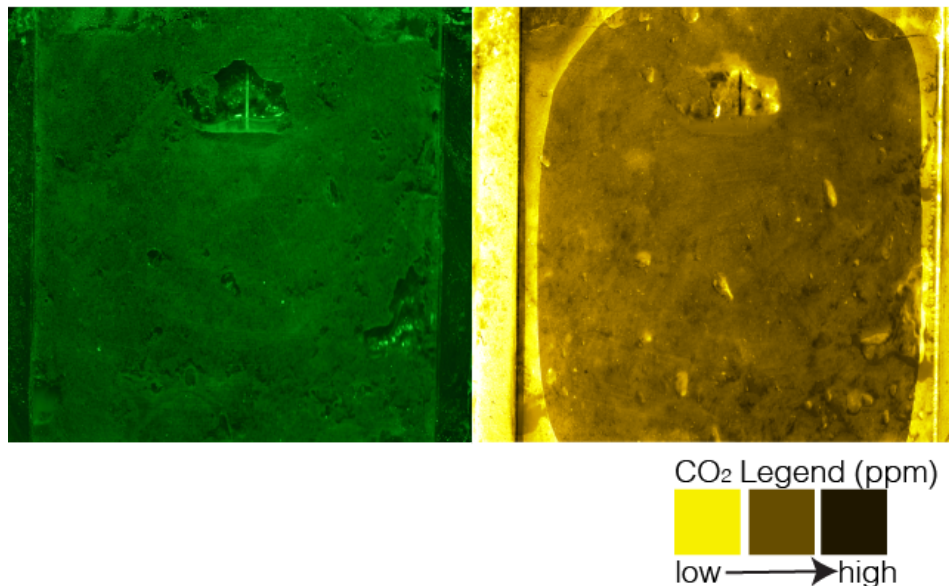
Figure 7. A comparison of R4 visible image to fluorescent ratio image. The visible image appears on the left and the ratio image appears on right. Both taken from time point 0, these images depict the same structures. The microdialysis probe is visible in the upper-center of the image encased. The CO$_2$ legend can be used to interpret the dynamics of the ratio image on the right.

The large air pocket may have both diffused and vented away the carbon dioxide

produced by microbes, diluting their potential effect. The most likely explanation is failure of

the probe in this replicate. Therefore future work with these probes requires positive testing

at the outset to validate that the probes are functioning as expected.

and vented away the carbon dioxide produced by microbes, diluting their potential effect.

In the rhizoboxes, certain soil structures showed either increased or decreased pixel

ratios that appeared to be uncorrelated with changes in carbon dioxide dynamics (Fig. 7). For

example, soil divots in the soil profile appear to be lighter in hue on the right-most side of the

box and shadowed on the left (Fig. 7). This could be explained by the wall effect— a

phenomena observed in the application of traditional planar optodes where an analyte of

interest may be underrepresented if its region of production is further from the planar optode

or overrepresented if the region of production is nearer to the planar optode (Li et al., 2019).

It is difficult to discern whether the apparently different carbon dioxide dynamics are a

function of proximity to the wall, or the actual curvature of the structures of interest, or both.

Though the rhizo-system appears to visualize pCO_2 shifts in different regions of the

rhizobox well by capturing macro-scale and micro-scale dynamics, inconsistencies with

respect to the soil structure hinder the application of this method. While this application of

HPTS is more soil-associated than planar optodes, fluorescent imaging only represented the

topmost layer of soil. Gas dynamics though are representative of the 3-dimensional nature of

soil because gases vent through macro and micro pores. Thus, dynamics visualized via the

HPTS fluorophore may represent unseen soil regions and not the regions of interest at the

topmost layer. While the potential of HPTS to help visualize soil dynamics synergizes

seamlessly with microdialysis technology, the limitations of the method need to be carefully considered before application.

4.   Conclusion

Because of increased carbon inputs, rhizosphere processes are nuanced and fast-changing at micro-scales. Development of technologies to address the complexities of studying this system has been slow, and the technologies have often interfered in appreciable ways with the contexts they aim to study (König et al., 2022). The aim of this study was to evaluate a novel application of microdialysis and the fluorophore HPTS together to simulate and visualize rhizosphere dynamics, respectively. Microbial activity was successfully stimulated via the microdialysis system in three out of four replicates, while controls showed no evidence of significant microbial activity around the probe. Subsequently, spatial patterns of pCO_2 around the microdialysis probe and throughout the rhizobox were observed through ratiometric analysis of the HPTS driven fluorescence images. This investigation uncovered a limitation of the method: pCO_2 artifacts emerged around certain spatial structures, possibly a function of their curvature and thus the way they reflected light, or the wall-effect. Perhaps, if a simpler media were used, substrate heterogeneity could be minimized so that artifacts could be more easily examined. Despite this limitation, merging microdialysis and HPTS driven fluorescence into one system appears to be a promising, nondestructive, high resolution method to study rhizosphere dynamics. In this proof-of-concept study we were able to successfully drive microbial activity *in situ* with microdialysis and visualize subsequent micro-scale microbial activity through spatial analysis of pCO_2. The successful recreation of microbial dynamics and spatial analysis with microdialysis and HPTS respectively is

25

suggestive of the viability of this method to recreate and explore rhizosphere processes. Future studies can use the method outlined in this thesis to better understand specific rhizosphere mechanisms that influence SOM turnover rates and soil C stocks as a whole.

References:

Alford, R., Simpson, H. M., Duberman, J., Hill, G. C., Ogawa, M., Regino, C., Kobayashi, H., & Choyke, P. L. (2009). Toxicity of organic fluorophores used in molecular imaging: Literature review. *Molecular Imaging*, *8*(6), 7290.2009.00031.

Bardgett, R. D., Mommer, L., & De Vries, F. T. (2014). Going underground: root traits as drivers of ecosystem processes. *Trends in Ecology & Evolution*, *29*(12), 692–699.

Baveye, P. C., Otten, W., Kravchenko, A., Balseiro-Romero, M., Beckers, É., Chalhoub, M., Darnault, C., Eickhorst, T., Garnier, P., Hapca, S., Kiranyaz, S., Monga, O., Mueller, C. W., Nunan, N., Pot, V., Schlüter, S., Schmidt, H., & Vogel, H.-J. (2018). Emergent properties of microbial activity in heterogeneous soil microenvironments: Different research approaches are slowly converging, yet major challenges remain. *Frontiers in Microbiology*, *9*, 1929.

Blagodatsky, S. A., Heinemeyer, O., & Richter, J. (2000). Estimating the active and total soil microbial biomass by kinetic respiration analysis. *Biology and Fertility of Soils*, *32*(1), 73–81.

Blagodatsky, S., Blagodatskaya, E., Yuyukina, T., & Kuzyakov, Y. (2010). Model of apparent and real priming effects: Linking microbial activity with soil organic matter decomposition. *Soil Biology and Biochemistry*, *42*(8), 1275–1283.

Blossfeld, S., Gansert, D., Thiele, B., Kuhn, A. J., & Lösch, R. (2011). The dynamics of oxygen concentration, pH value, and organic acids in the rhizosphere of Juncus spp. *Soil Biology and Biochemistry*, *43*(6), 1186–1197.

Brackin, R., Atkinson, B. S., Sturrock, C. J., & Rasmussen, A. (2017). Roots-eye view: Using microdialysis and microCT to non-destructively map root nutrient depletion and

accumulation zones (Vol. 40, No. 12, pp. 3135-3142).

Buckley, S., Brackin, R., Jämtgård, S., Näsholm, T., & Schmidt, S. (2020). Microdialysis in soil environments: Current practice and future perspectives. *Soil Biology and Biochemistry*, *143*, 107743.

Canarini, A., Kaiser, C., Merchant, A., Richter, A., & Wanek, W. (2019). Root exudation of primary metabolites: mechanisms and their roles in plant responses to environmental stimuli. *Frontiers in Plant Science*, *10*, 157.

Carminati, A., Benard, P., Ahmed, M. A., & Zarebanadkouki, M. (2017). Liquid bridges at the root-soil interface. *Plant and Soil*, vol. 417, no. 1-2, Aug. 2017.

C. Mondini, M. Cayuela (2006). Soil microbial biomass activation by trace amounts of readily available substrate. *Biology and Fertility of Soils.*

Chen, R., Senbayram, M., Blagodatsky, S., Myachina, O., Dittert, K., Lin, X., Blagodatskaya, E., & Kuzyakov, Y. (2014). Soil C and N availability determine the priming effect: Microbial N mining and stoichiometric decomposition theories. *Global Change Biology*, *20*(7), 2356–2367.

Chen, X., & Hu, Q. (2004). Groundwater influences on soil moisture and surface evaporation. *Journal of Hydrology*, *297*(1–4), 285–300.

Clarholm, M. (1981). Protozoan grazing of bacteria in soil—impact and importance. *Microbial Ecology, 7, v. 343-350(4)*

de Graaff, M., Classen, A. T., Castro, H. F., & Schadt, C. W. (2010). Labile soil carbon inputs mediate the soil microbial community composition and plant residue decomposition rates. *New Phytologist, 188*(4), 1055–1064.

Demand, D., Schack-Kirchner, H., & Lang, F. (2017). Assessment of diffusive phosphate supply in soils by microdialysis. *Journal of Plant Nutrition and Soil Science*, *180*(2), 220–230.

Dijkstra, F. A., Carrillo, Y., Pendall, E., & Morgan, J. A. (2013). Rhizosphere priming: A nutrient perspective. *Frontiers in Microbiology*, *4*.

Dowdy, Kelsey (2021). Reframing plant invasion: Altered watershed biogeochemistry as a cause and consequence of giant reed Arundo donax. Accession No. 28541873, University of California, Santa Barbara, ProQuest Dissertations Publishing.

Enick, R. M., & Klara, S. M. (1990). CO2 solubility in water and brine under reservoir conditions. *Chemical Engineering Communications*, *90*(1), 23-33.

Ettema, C. (2002). Spatial soil ecology. *Trends in Ecology & Evolution*, *17*(4), 177–183.

Fierer, N., Schimel, J. P., Cates, R. G., & Zou, J. (2001). Influence of balsam poplar tannin fractions on carbon and nitrogen dynamics in Alaskan taiga floodplain soils. *Soil Biology*.

Fontaine, S., Mariotti, A., & Abbadie, L. (2003). The priming effect of organic matter: A question of microbial competition? *Soil Biology and Biochemistry*, *35*(6), 837–843.

Garcia, C., Roldan, A., & Hernandez, T. (2005). Ability of different plant species to promote microbiological processes in semiarid soil. *Geoderma*, *124*(1–2), 193–202.

Gochun, V. L. (1988). An estimation of microbial death rate and limitations of N or C during wheat straw decomposition. *Soil Biol. Biochemistry Vol. 20, No. 3*. 293-298

Grossmann, J., & Udluft, P. (1991). The extraction of soil water by the suction-cup method: A review. *Journal of Soil Science*, *42*(1), 83–93.

Henry, William (1802). Experiments on the quantity of gases absorbed by water, at different temperatures, and under different pressures. *Royal Society Publishing.*

Hicks Pries, C. E., Logtestijn, R. S. P., Schuur, E. A. G., Natali, S. M., Cornelissen, J. H. C., Aerts, R., & Dorrepaal, E. (2015). Decadal warming causes a consistent and persistent shift from heterotrophic to autotrophic respiration in contrasting permafrost ecosystems. *Global Change Biology*, *21*(12), 4508–4519.

Hobbie, J. E., & Hobbie, E. A. (2013). Microbes in nature are limited by carbon and energy: The starving-survival lifestyle in soil and consequences for estimating microbial rates. *Frontiers in Microbiology*, *4*.

Holz, M., Becker, J. N., Daudin, G., & Oburger, E. (2020). Application of planar optodes to measure CO2 gradients in the rhizosphere of unsaturated soils. *Rhizosphere*, *16*, 100266.

Homyak, P.M., Slessarev, E.W., Hagerty, S., Greene, A.C., Marchus, K., Dowdy, K., Iverson, S. and Schimel, J.P. (2021), Amino acids dominate diffusive nitrogen fluxes across soil depths in acidic tussock tundra. *New Phytologist*, 231: 2162-2173.

Inselsbacher, E., Oyewole, O. A., & Näsholm, T. (2014). Early season dynamics of soil nitrogen fluxes in fertilized and unfertilized boreal forests. *Soil Biology and Biochemistry*, *74*, 167–176.

Johnson, K. M., Hughes, J. E., Donaghay, P. L., & Sieburth, J. M. (1990). Bottle-calibration static head space method for the determination of methane dissolved in seawater. *Analytical Chemistry*, *62*(21), 2408–2412.

Kaye, J., Barrett, J., & Burke, I. (2002). Stable Nitrogen and Carbon pools in grassland soils of variable texture and carbon content. *Ecosystems*, *5*(5), 461–471.

Keenan, S. W., Schaeffer, S. M., Jin, V. L., & DeBruyn, J. M. (2018). Mortality hotspots: Nitrogen cycling in forest soils during vertebrate decomposition. *Soil Biology and Biochemistry*, *121*, 165–176.

Kho, C. M., Enche Ab Rahim, S. K., Ahmad, Z. A., & Abdullah, N. S. (2017). A review on microdialysis calibration methods: The theory and current related efforts. *Molecular Neurobiology*, *54*(5), 3506–3527.

König, A., Wiesenbauer, J., Gorka, S., Marchand, L., Kitzler, B., Inselsbacher, E., & Kaiser, C. (2022). Reverse microdialysis: A window into root exudation hotspots. *Soil Biology and Biochemistry*, *174*, 108829.

Kraus, T. E. C., Zasoski, R. J., Dahlgren, R. A., Horwath, W. R., & Preston, C. M. (2004). Carbon and nitrogen dynamics in a forest soil amended with purified tannins from different plant species. *Soil Biology and Biochemistry*, *36*(2), 309–321.

Kuzyakov, Y. (2002). Review: Factors affecting rhizosphere priming effects. *Journal of Plant Nutrition and Soil Science*, *165*(4), 382–396.

Kuzyakov, Y. (2010). Priming effects: Interactions between living and dead organic matter. *Soil Biology and Biochemistry*, *42*(9), 1363–1371.

Kuzyakov, Y., & Blagodatskaya, E. (2015). Microbial hotspots and hot moments in soil: Concept & review. *Soil Biology and Biochemistry*, *83*, 184–199.

Kuzyakov, Y., Friedel, J. K., & Stahr, K. (2000). Review of mechanisms and quantification of priming effects. *Soil Biology and Biochemistry*, *32*(11–12), 1485–1498.

Kuzyakov, Y., & Razavi, B. S. (2019). Rhizosphere size and shape: Temporal dynamics and spatial stationarity. *Soil Biology and Biochemistry*, *135*, 343–360.

Lauber, C. L., Strickland, M. S., Bradford, M. A., & Fierer, N. (2008). The influence of soil properties on the structure of bacterial and fungal communities across land-use types. *Soil Biology and Biochemistry*, *40*(9), 2407–2415.

Lenzewski, N., Mueller, P., Meier, R.J., Liebsch, G., Jensen, K. and Koop-Jakobsen, K.

(2018), Dynamics of oxygen and carbon dioxide in rhizospheres of *Lobelia dortmanna* – a

planar optode study of belowground gas exchange between plants and sediment. New Phytol,

218: 131-141.

Li, C., Ding, S., Yang, L., Zhu, Q., Chen, M., Tsang, D. C. W., Cai, G., Feng, C., Wang, Y., &

Zhang, C. (2019). Planar optode: A two-dimensional imaging technique for studying

spatial-temporal dynamics of solutes in sediment and soil. *Earth-Science Reviews*, *197*,

102916.

Polerecky, L., Volkenborn, N., & Stief, P. (2006). High temporal resolution oxygen imaging

in bioirrigated sediments. *Environmental Science & Technology*, *40*(18), 5763–5769.

Randewig, D., Marshall, J. D., Näsholm, T., & Jämtgård, S. (2019). Combining microdialysis

with metabolomics to characterize the in situ composition of dissolved organic compounds in

boreal forest soil. *Soil Biology and Biochemistry*, *136*(July), 107530–107530.

Rasmussen, C., Heckman, K., Wieder, W. R., Keiluweit, M., Lawrence, C. R., Berhe, A. A.,

Blankinship, J. C., Crow, S. E., Druhan, J. L., Hicks Pries, C. E., Marin-Spiotta, E., Plante,

A. F., Schädel, C., Schimel, J. P., Sierra, C. A., Thompson, A., & Wagai, R. (2018). Beyond

clay: Towards an improved set of variables for predicting soil organic matter content.

Biogeochemistry, *137*(3), 297–306.

Ronn, R., Griffith, B. S., Ekelund, F., & Christensen, S. (2022). Spatial distribution and

successional pattern of microbial activity and micro-faunal populations on decomposing.

Schimel, J. (2003). The implications of exoenzyme activity on microbial carbon and nitrogen

limitation in soil: A theoretical model. *Soil Biology and Biochemistry*, *35*(4), 549–563.

Seaton, F. M., George, P. B. L., Lebron, I., Jones, D. L., Creer, S., & Robinson, D. A. (2020).

Soil textural heterogeneity impacts bacterial but not fungal diversity. *Soil Biology and Biochemistry*, *144*, 107766.

Silver, W. L., Neff, J., McGroddy, M., Veldkamp, E., Keller, M., & Cosme, R. (2000). Effects of soil texture on belowground carbon and nutrient storage in a lowland amazonian forest ecosystem. *Ecosystems*, *3*(2), 193–209.

Smercina, D. N., Bailey, V. L., & Hofmockel, K. S. (2021). Micro on a macroscale: Relating microbial-scale soil processes to global ecosystem function. *FEMS Microbiology Ecology*, *97*(7), fiab091.

Spohn, M., & Kuzyakov, Y. (2013). Distribution of microbial- and root-derived phosphatase activities in the rhizosphere depending on P availability and C allocation – coupling soil zymography with 14C imaging. *Soil Biology and Biochemistry*, *67*, 106–113.

Sulman, B. N., Phillips, R. P., Oishi, A. C., Shevliakova, E., & Pacala, S. W. (2014). Microbe-driven turnover offsets mineral-mediated storage of soil carbon under elevated CO2. *Nature Climate Change*, *4*(12), 1099–1102.

Ushio, M., Balser, T. C., & Kitayama, K. (2013). Effects of condensed tannins in conifer leaves on the composition and activity of the soil microbial community in a tropical montane forest. *Plant and Soil*, *365*(1–2), 157–170.

Vance, E. D., & Chapin III, F. S. (2001). Substrate limitations to microbial activity in taiga forest floors. *Soil Biology and Biochemistry*, *33*(2), 173–188.

Vogel, L. E., Makowski, D., Garnier, P., Vieublé-Gonod, L., Coquet, Y., Raynaud, X., Nunan, N., Chenu, C., Falconer, R., & Pot, V. (2015). Modeling the effect of soil meso- and macropores topology on the biodegradation of a soluble carbon substrate. *Advances in Water Resources*, *83*, 123–136.

Zhu, Q., Aller, R. C., & Fan, Y. (2006). A new ratiometric, planar fluorosensor for measuring high resolution, two-dimensional pCO2 distributions in marine sediments. *Marine Chemistry*, *101*(1–2), 40–53.